Interplay between magnetic structures and surface states in $MnBi_2Te_4$ from first-principles studies

Zujian Dai, Gan Jin, and Lixin He*

CAS Key Laboratory of Quantum Information, University of Science and Technology of China, Hefei 230026, China and Synergetic Innovation Center of Quantum Information and Quantum Physics, University of Science and Technology of China, Hefei 230026, China

(Received 25 October 2022; revised 7 July 2023; accepted 21 July 2023; published 10 August 2023)

The antiferromagnetic topological insulator $MnBi_2Te_4$ was believed to have a topological surface state (TSS) with large band gap due to the ferromagnetic (FM) order on the surface and to be able to host the long-sought axion states. However, recent angle-resolved photoemission spectroscopy experiments indicate that the TSS is gapless, contradicting the theoretical predictions. Meanwhile, several experiments have suggested that there is robust out-of-plane FM order on the surface of $MnBi_2Te_4$. To understand these seemingly contradictory results, we carry out comprehensive first-principles calculations to investigate the interplay between the surface magnetism and the TSS. Our calculations provide direct evidence that in a wide range of parameters, the (nearly) gapless TSS can coexist with the surface FM order, therefore solving the paradox of the surface magnetism and the gapless TSS. We further show that proximity effects can be a promising route to open the gap in the TSS of $MnBi_2Te_4$. Our research deepens the understanding of the relationship between surface magnetism and TSSs.

DOI: 10.1103/PhysRevB.108.085112

I. INTRODUCTION

The interplay between magnetism and nontrivial band topology may lead to rich physical phenomena that not only are interesting for fundamental physics but also have important potential applications in spintronic devices [1,2]. Therefore $MnBi_2Te_4$, the first synthesized intrinsic magnetic topological insulator (MTI) [3–5], has attracted great attention since its appearance [6–10]. $MnBi_2Te_4$ has an A-type antiferromagnetic (AFM) structure, which enables unique thickness-dependent topological properties: For a thin film with an odd number of layers, it is a quantum anomalous Hall (QAH) insulator [11–15], whereas for a thin film with an even number of layers, it is the long-sought axion insulator [9,13,14,16–24].

However, despite intensive research, the nature of the topological surface states (TSSs) of this material is still very controversial [6,18,25–38]. First-principles calculations predicted that $MnBi_2Te_4$ has a TSS with a considerable energy gap (larger than 60 meV) due to the ferromagnetic (FM) spin order on the surface [6,8,9,25–27], which is promising for achieving a QAH state at rather high temperatures. Nevertheless, the zero-field QAH effect (QAHE) was observed only at rather low temperatures (below 1.6 K) in this system [12,13]. A gapped TSS was reported in early angle-resolved photoemission spectroscopy (ARPES) experiments [6,25–27]. However, more recent ARPES measurements have observed a nearly perfect Dirac cone or a strong reduction in the gap at the Dirac point on the $MnBi_2Te_4$ (0001) surface [18,28–36,38].

To understand the origin of the gapless TSS [37], three scenarios have been proposed, including surface magnetic reconstruction [18,29,31,39], geometric reconfiguration [36,40–43], and hybridization of the surface and bulk bands [44,45]. For surface magnetic reconstruction, it has been shown that three types of surface spin reorientation may lead to gapless TSSs, including paramagnetism (PM), in-plane A-type AFM, and G-type AFM [29]. However, both time-resolved ARPES [32] and magnetic force microscopy [46] have suggested that there is robust out-of-plane FM order on the surface of $MnBi_2Te_4$. A key perplexity here is whether the gapless TSSs can coexist with surface FM order [32].

In this paper, we carry out comprehensive first-principles calculations to investigate the interplay between the surface magnetism and the TSS. Our calculations provide solid evidence that in a wide range of parameters, the (nearly) gapless TSSs can coexist with the surface FM order, therefore solving the paradox concerning the coexistence of surface magnetism and a gapless TSS. We explore the underlying mechanisms for the emergence of these almost gapless TSSs. We further show that proximity effects can be a promising route to open the gap in the TSSs of $MnBi_2Te_4$.

II. COMPUTATIONAL DETAILS

The first-principles calculations are carried out with the Atomic-Orbital Based *Ab-Initio* Computation at USTC (ABACUS) code [47,48]. The Perdew-Burke-Ernzerhof (PBE) [49] exchange-correlation functional is adopted, and the density functional theory with dispersion correction DFT-D3 is used to account for the van der Waals (vdW) interactions [50]. A Hubbard-like U value of 4.0 eV is used for the half-filled, strongly localized Mn $3d$ orbitals [51,52]. The essential results remain unchanged when employing different reasonable U values. The ABACUS code is developed to perform large-scale density functional theory calculations based

*helx@ustc.edu.cn

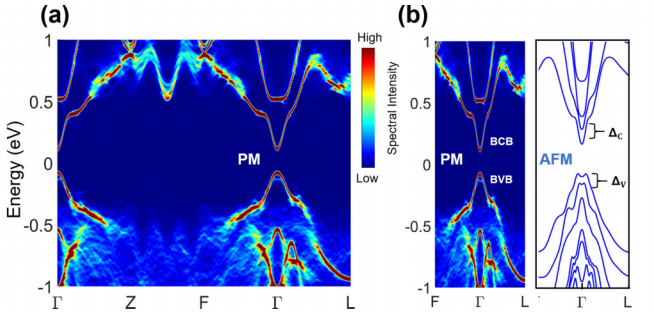

FIG. 1. (a) The unfolded band spectra of $MnBi_2Te_4$ in the PM phase. (b) Comparison of unfolded band spectra of $MnBi_2Te_4$ in the PM and A-type AFM phases around the Γ point. The color shows the spectra intensity, which is broadened by 4 meV. BCB and BVB denote the bulk conduction bands and bulk valence bands, respectively. The energy band splitting of BCBs and BVBs in the AFM phase is denoted by Δ_C and Δ_V, respectively.

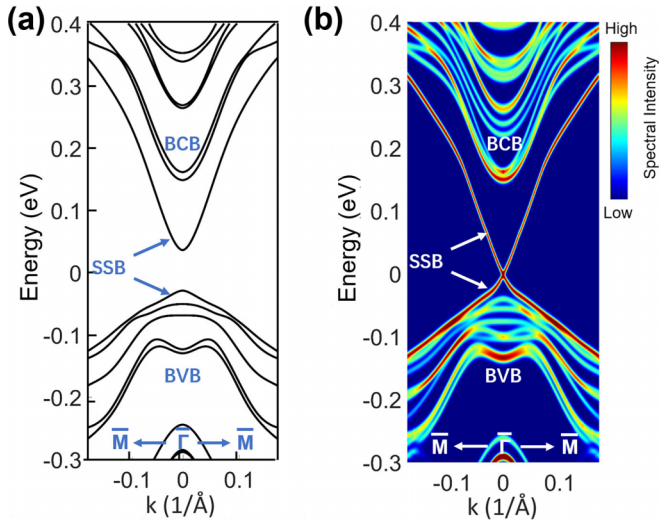

FIG. 2. (a) The band structure of the $1 \times 1 \times 6$ AFM slab. (b) The unfolded band spectra of the $4 \times 4 \times 6$ PM slab. The color shows the intensity of the unfolded band spectra, which is broadened by 4 meV. SSB, BCB, and BVB denote the surface-state bands, bulk conduction bands, and bulk valence bands, respectively.

on numerical atomic orbitals (NAOs) [47]. The optimized norm-conserving Vanderbilt (ONCV) [53] fully relativistic pseudopotentials [54] from the PSEUDODOJO library [55] are used. The valence electrons for Mn, Bi, and Te are $3s^2 3p^6 3d^5 4s^2$, $5d^{10} 6s^2 6p^3$, and $4d^{10} 5s^2 5p^4$, respectively, and the NAO bases for Mn, Bi, and Te are $4s2p2d1f$, $2s2p2d$, and $2s2p2d$, respectively. In the self-consistent and band structure calculations, the energy cutoff for the wave functions is set to 120 Ry. Experimental lattice parameters [56] have been used. The atomic positions are fully optimized until all forces are less than 0.01 eV/Å.

III. RESULTS AND DISCUSSION

A. Band structures of bulk $MnBi_2Te_4$ in AFM and paramagnetic phases

The $MnBi_2Te_4$ has a vdW stacking structure (space group $R\bar{3}m$) with a MnTe bilayer sandwiched by Bi_2Te_3. The unit cell consists of a Te-Bi-Te-Mn-Te-Bi-Te septuple layer (SL) [27,57,58]. Below the Néel temperature $T_N = 25$ K, the spins within each SL are found to be parallel to the out-of-plane easy axis but antiparallel within the adjacent SLs [6,27,58,59]. The conduction and valance band splittings in $MnBi_2Te_4$ below the Néel temperature were reported, due to the spins ordering below the Néel temperature [28,45].

We first examine the impact of magnetism on the bulk band structures, by comparing the band structures of $MnBi_2Te_4$ in the PM and A-type AFM phases. To simulate the band structure of the bulk $MnBi_2Te_4$ in the PM phase, we construct a $4 \times 4 \times 4$ supercell. The Ising-like spins on Mn ions [60] are randomly initialized. We neglect the structure relaxation due to different spin configurations.

The band structures calculated in the supercell are unfolded to the nonmagnetic unit cell [61,62]. We find that the unfolded band structures of different random spin configurations are almost the same, which suggests that the supercell is large enough to describe the PM state. The unfolded band structures of the PM phase are shown in Fig. 1(a), which shows a sharp and well-defined band spectra around the Γ point. However, the bands become blurred around the Z and F points. This is because around the Γ point, where the Bloch states have a long wavelength, the spin configurations are well averaged within the wavelength range. In contrast, when the wavelength of the Bloch states is short, the short-range spin fluctuation blurs the band structure.

The band structures of $MnBi_2Te_4$ in the PM phase around the Γ point are compared with those in the AFM phase in Fig. 1(b). In addition to some differences in details, there is a significant difference between the AFM bands and PM bands, i.e., the highest valence band and the lowest conduction bands of PM states split into two bands in the AFM states. The energy splitting of the conduction band minimum (CBM) is approximately 90 meV, which is larger than that from ARPES experiments [28] (50 meV at 7.5 K). The difference might come from the fact that the magnetic state near the surface is not perfectly AFM in experiments.

B. Band structures of surface states

We now turn to the surface states of $MnBi_2Te_4$ under different magnetizations. We construct a slab containing $4 \times 4 \times 6$ $MnBi_2Te_4$ unit cells. There are 96 Mn atoms in the slab. We change the spin orientations of Mn ions in the slab to realize different magnetic configurations. A 15-Å vacuum is added to avoid the interactions between the slab and its periodic images. The atomic positions of the slab are relaxed under the A-type AFM configuration.

The band structure of the perfect A-type AFM $MnBi_2Te_4$ slab is shown in Fig. 2(a). We determine the surface states by analyzing the real space distributions of the wave functions. The surface state has a considerable gap of 65 meV, which is consistent with previous theoretical results [6,8,9,25–27].

When the temperature is above the Néel temperature, the experiment shows that $MnBi_2Te_4$ becomes PM and shows gapless surface states. It has been predicted that the PM $MnBi_2Te_4$ is a strong topological insulator with a gapless TSS in the (0001) direction [10,28]. We calculate the (unfolded)

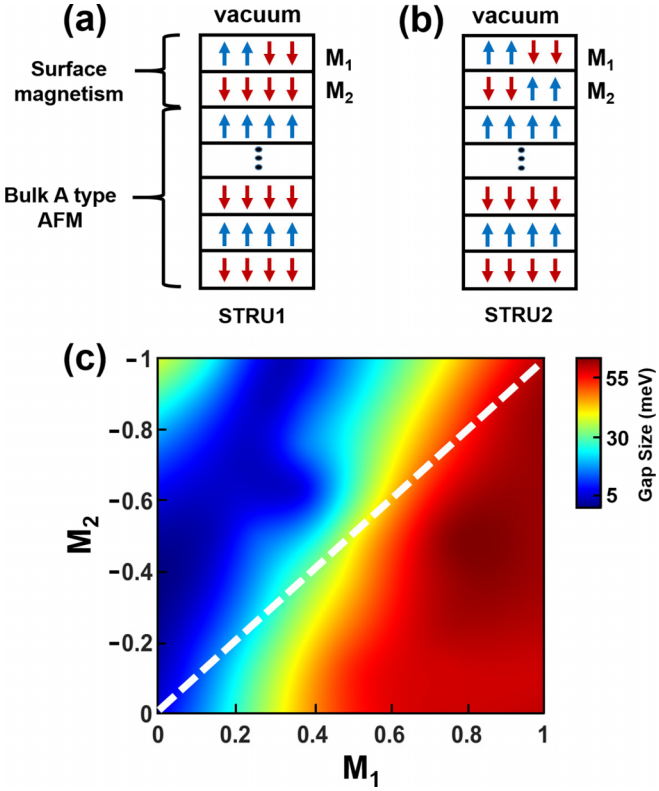

FIG. 3. (a) and (b) Illustrations of two different surface magnetic reconstructions (STRU1 and STRU2): The first SL is PM, i.e., $M_1 = 0$ (a); both the first SL and the second SL are PM, i.e., $M_1 = M_2 = 0$ (b). (c) The band gap of the TSS under different surface magnetizations M_1 and M_2. The color shows the size of the gap. The white dashed line is the guideline for $M_1 = -M_2$.

band structures of the PM slab, which are shown in Fig. 2(b). As expected, the unfolded spectra of the PM slab show a gapless TSS with a bright Dirac point. We find that the surface states are mostly localized on the outermost two layers, which is consistent with model Hamiltonian calculations [40]. Therefore one may expect that the magnetism of the top two SLs may have a great influence on the TSS.

Previous theoretical investigations suggested that the gapped surface states in the AFM $MnBi_2Te_4$ may protect the axion states [9,13,14,21–24]. However, experimentally, it has been found that the surface states of $MnBi_2Te_4$ are gapless even below the Néel temperature, which contradicts the theoretical predictions. The origin of the gapless surface states is under intensive discussion [18,28–38]. It has been suggested that the gapless TSS may come from the magnetic reconstructions at the surface. To understand the surface states in $MnBi_2Te_4$, we calculate the surface states under different surface magnetizations.

We first calculate the surface states on a system in which all layers are in the A-AFM state except the top SL, which is PM, as sketched in Fig. 3(a). We focus on the TSS of the top surface, which can be easily identified by its localization. We find that the TSS of the top surface is gapped by approximately 38 meV, slightly larger than half of the gap of the ideal FM surface. This is because the TSSs are most localized on the first two SLs of the surface [62] and the FM order in the second SL still has a large effect on the TSS, which opens the gap. To examine this idea, we calculate the TSS of the system where the top two SLs of the slab are set to PM as sketched in Fig. 3(b). Indeed, the band gap of the TSS of the top surface is approximately 0.6 meV, which is too small to be detected experimentally. These results suggest that we must consider the magnetic reconstructions of the first two SLs to understand the TSS.

To obtain a more general understanding of the relationship between the surface magnetism and the TSS, we systematically calculate the TSS of systems with different magnetizations of the top two SLs. The surface magnetic reconstruction has several possible microscopic origins. For example, it may come from the competition of the magnetic interactions of Mn layers [60], or it may come from the native point defects in $MnBi_2Te_4$ [36,38,42]. It may also come from the domain wall structures of $MnBi_2Te_4$ [46]. In this paper, we do not discuss the mechanisms of the magnetic reconstructions, which would be an interesting topic for future investigations.

We define the layer magnetization of each SL as

$$M_i = \frac{N_{i,\uparrow} - N_{i,\downarrow}}{N_{i,\uparrow} + N_{i,\downarrow}}, \tag{1}$$

where $N_{i,\uparrow}$ ($N_{i,\downarrow}$) is the total number of up (down) spins in the ith SL. Because the interlayer exchange interactions are AFM-like, we set the layer magnetizations M_1 and M_2 to have opposite signs. The value of the TSS gap as a function of layer magnetizations M_1 and M_2 is shown in Fig. 3(c). When both M_1 and M_2 are zero (i.e., they are both PM), the band gap is approximately zero, whereas when $M_1 = -M_2 = 1$ (i.e., perfect A-type AFM), the energy gap of TSS is approximately 65 meV. Remarkably, when $|M_2|$ is larger than $|M_1|$, the surface states tend to have very small band gaps. Especially around $M_1 \approx -\frac{1}{3}M_2$, the band gap of TSS is nearly zero. In general, there is a large region in which the energy gap size is tiny. In this region, the total surface magnetization $M_1 + M_2 < 0$, i.e., there is net FM magnetization. Interestingly, when $M_1 + M_2 = 0$, i.e., the white dashed line in Fig. 3(c), the band gap of TSS is not necessarily zero, which increases with increasing M_1. When $|M_1| > M_2|$, the TSS tends to have a large gap. Especially near $M_1 = 0.8$, $M_2 = -0.45$, the gap is approximately 69 meV, which is even slightly larger than that of the perfect A-type AFM slab. Because M_2 is in the inner layer, which is more affected by the bulk magnetism, it is highly plausible that the system is in the region $|M_2| > |M_1|$, where the TSS gap is small. These results may well explain why $MnBi_2Te_4$ has gapless surface states. The unfolded spectra of surface states under different surface magnetizations can be found in the Supplemental Material (SM) [62]. We also study the impact of the Coulomb U value on the gap of the surface states and find that it has little effect on the results. More details can be found in the SM [62].

C. Origin of the gapless surface states

We further analyze the numerical results from the previous section to investigate the origin of the gapless TSS. It is widely recognized that a surface with time-reversal symmetry exhibits a gapless TSS [10,28]. To understand the origin of

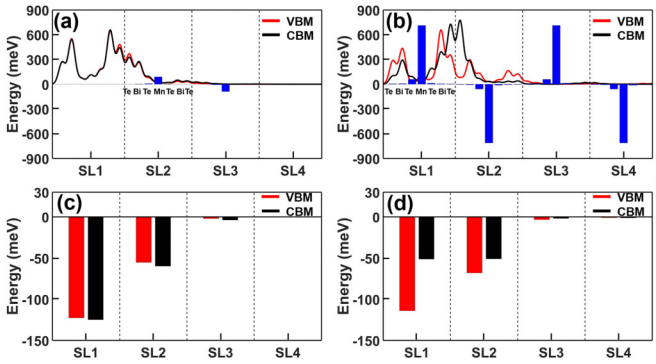

FIG. 4. (a) and (b) The exchange interaction strength (blue bars) and the spatial distribution of the TSS wave function localized on different atomic layers, for the surface magnetizations $(M_1, M_2) = (0, 0)$ (a) and $(M_1, M_2) = (1, -1)$ (b). (c) and (d) The reduction in band energy caused by the exchange interaction for both the VBM and the CBM, originating from different SL layers, for the surface magnetizations $(M_1, M_2) = (0, 0)$ (c) and $(M_1, M_2) = (1, -1)$ (d).

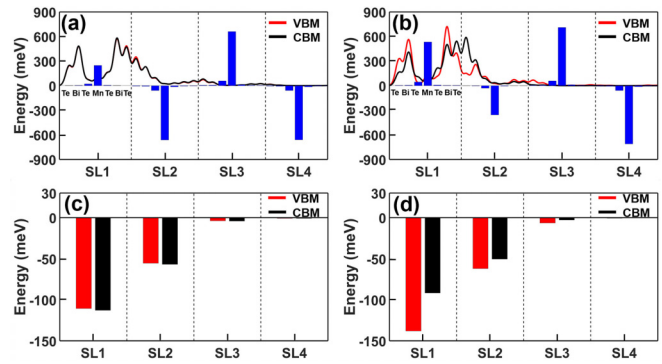

FIG. 5. (a) and (b) The exchange interaction strength (blue bars) and the spatial distribution of the TSS wave function localized on different atomic layers, for the surface magnetizations $(M_1, M_2) = (\frac{3}{8}, -1)$ (a) and $(M_1, M_2) = (\frac{3}{4}, -\frac{1}{2})$ (b). (c) and (d) The reduction in band energy caused by the exchange interaction for both the VBM and the CBM, originating from different SL layers, for the surface magnetizations $(M_1, M_2) = (\frac{3}{8}, -1)$ (c) and $(M_1, M_2) = (\frac{3}{4}, -\frac{1}{2})$ (d).

the TSS, we separate the Hamiltonian at the Γ point, which is expressed in NAO bases, into two distinct parts. The first part, H_{T}, preserves time-reversal symmetry, while the second part, H_{exc}, arises from the exchange interaction, i.e.,

$$H = H_{\mathrm{T}} + H_{\mathrm{exc}}, \tag{2}$$

and

$$H_{\mathrm{T}}(\sigma, \sigma')(\Gamma) = +H_{\mathrm{T}}(\bar{\sigma}, \bar{\sigma}')(\Gamma), \tag{3}$$

$$H_{\mathrm{exc}}(\sigma, \sigma')(\Gamma) = -H_{\mathrm{exc}}(\bar{\sigma}, \bar{\sigma}')(\Gamma), \tag{4}$$

where σ is the spin index and $\bar{\sigma} = -\sigma$. By decomposing the contribution of H_{exc} for each ion, we found that not surprisingly, the majority of the contribution originated from the Mn ions.

We first consider two specific surfaces: (1) $M_1 \approx M_2 \approx 0$ (PM) and (2) $M_1 = -M_2 = 1$ (AFM). The averaged exchange fields within each atomic layer for these cases are illustrated in Figs. 4(a) and 4(b), respectively. On the PM surface, where the first two SLs possess (approximate) time-reversal symmetry, the averaged exchange fields are close to zero. On the other hand, for the AFM case, the exchange fields are significantly larger, approximately 80 meV at each Mn layer. Furthermore, we depict the weight of the wave functions for the valence band maximum (VBM) and conduction band minimum (CBM) states. The TSSs primarily localize on the outermost two SLs, predominantly on the first SL. For the PM surface, the weights of the two wave functions are nearly identical due to the presence of time-reversal symmetry. In contrast, for the AFM surface, the two wave functions exhibit notable differences.

We further calculate the reduction in band energy of the TSS caused by the exchange fields [63–65], which is defined as $\Delta E_{\mathrm{exc}} = \langle \psi_{\mathrm{TSS}} | H_{\mathrm{exc}} | \psi_{\mathrm{TSS}} \rangle$, where ψ_{TSS} is the wave function of a TSS. The results for both the VBM and the CBM are shown in Figs. 4(c) and 4(d) for the PM and AFM surfaces, respectively. We further show the contribution to the reduction in band energy from different SLs. As we see, the first SL has a much larger contribution than the second SL. Interestingly, even though the *average* exchange fields are approximately zero on the PM surface, the exchange fields still have a substantial impact on both the valence and conduction bands, due to local exchange fields. However, the *overall* influence of the exchange fields affects the valence band and conduction band in the same manner, as they possess time-reversal symmetry in an average sense. Consequently, the gap remains approximately zero. On the other hand, for the perfect AFM surface states, the effective exchange fields have much larger effects on the VBM than on the CBM, as their wave functions differ significantly, and therefore open a considerable gap.

Figure 5 presents a comparison of the results for $(M_1, M_2) = (\frac{3}{8}, -1)$ and $(M_1, M_2) = (\frac{3}{4}, -\frac{1}{2})$. In the former case, the TSS exhibits an almost zero gap, while in the latter case, a large gap is observed. In Fig. 5(a) for $(M_1, M_2) = (\frac{3}{8}, -1)$, the weight of the wave functions is quite similar for the VBM and CBM states. Consequently, despite the presence of significant exchange fields that result in a reduction in band energies for both the VBM and CBM states, the reductions are very close to each other. Thus the band gap remains very small. In contrast, for $(M_1, M_2) = (\frac{3}{4}, -\frac{1}{2})$, the wave functions exhibit substantial differences, as shown in Fig. 5(b). Consequently, the exchange fields have a much larger effect on the VBM state compared with the CBM state, as illustrated in Fig. 5(c). This significant difference in the impact of the exchange fields leads to a considerable band gap. These results demonstrate that the band gap of a TSS is determined by the difference in the effects of the exchange fields on the VBM and CBM. When the exchange fields have similar influences on both states, the band gap remains small. However, when the exchange fields have distinct effects on the VBM and CBM states, a significant band gap arises in the TSS.

According to our calculations, the magnetization of the surface layers does not have to be zero to have a (nearly) gapless TSS. The magnetization of the first SL might be weakened by dangling bonds or defects [33,36,38,66] and is much weaker than that of the second SL. Therefore the first two SLs could still have large net FM magnetization, while the gap of

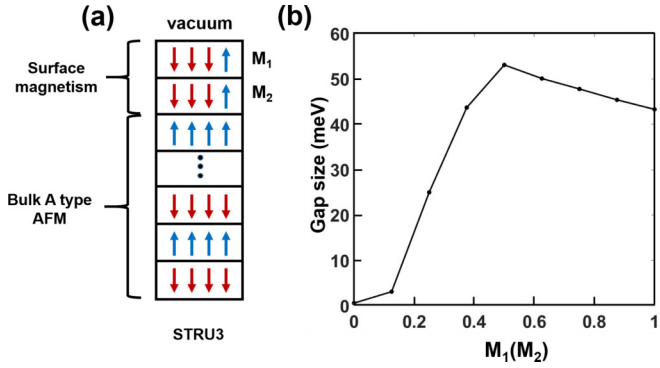

FIG. 6. (a) Illustration of the magnetic configuration with changes in the magnetization of the first two layers and setting $M_1 = M_2$. (b) The TSS band gap as a function of the surface magnetization $M_1 = M_2$.

the TSS is nearly zero. This scenario is different from previous works, where the magnetic reconstruction leads to zero magnetization on the surface [18,31,39]. Our results provide direct evidence that the gapless TSS may coexist with the FM order on the surface [46,60]. These results also suggest that the interaction between the TSS and surface magnetism is too complex to be described well by simple effective models, and atomistic models are necessary to obtain quantitative results.

We note that the A-type AFM configuration still has the lowest total energy if the slab has perfect crystal structure. However, it has been shown that there are several types of defects on the surface, e.g., the existence of cation (Mn-Bi) intermixing [38], which may weaken the magnetization of the surface. It is plausible to expect that the outermost SL may contain more defects, which could explain why the system falls into the parameter region described in Ref. [38] (which covers a relatively large parameter space) where the magnetization of the second SL is greater than that of the first. However, to gain a complete understanding of this phenomenon, it is crucial to identify the specific types of defects present on the surface, which is beyond the scope of the current study. Nonetheless, this presents a promising direction for future research.

D. How to get gapped surface states

To realize the QAH effect and axion insulators, we need to open a considerable gap in the TSS. A promising way to open the gap is to polarize the spins of the outermost layers using proximity effects. To study the relation between the spin polarization and the TSS band gap in this case, we calculate the band structures using the spin configurations shown in Fig. 6(a), i.e., the first two SLs are polarized along the same direction. To simplify the discussion, we assume $M_1 = M_2$. The calculated band gap as a function of M_1 is shown in Fig. 6(b). The TSS gap first increases with increasing M_1 and is saturated at $M_1 = 0.5$, with a TSS gap of 55 meV. The gap decreases slightly when further increasing M_1. The decrease in the TSS gap may come from the tendency to become a Weyl semimetal [8,9,67] when all spins are polarized in the same direction, i.e., a FM state. In practice, M_1 could be larger than M_2, or even have the opposite sign of M_2, because the first SL is closer to the magnetic materials, but according to Fig. 3(c), we could still expect that the TSS may have a considerable band gap. Therefore the heterojunction technique and the proximity effect form a promising route to open a robust gap in $MnBi_2Te_3$ [68–72].

IV. SUMMARY

We carry out a comprehensive investigation of the interplay between the surface states and the magnetism of $MnBi_2Te_4$. Our calculations provide direct evidence that in a wide range of parameters, the gapless (or heavily reduced gap) TSS can coexist with the surface FM order. We further show that proximity effects can be a promising route to open the gap of the TSS of $MnBi_2Te_4$. Our research deepens the understanding of the relationship between surface magnetism and the TSS.

ACKNOWLEDGMENTS

This work was funded by Chinese National Science Foundation Grant No. 12134012. The numerical calculations were performed on the USTC HPC facilities.

[1] L. Šmejkal, Y. Mokrousov, B. Yan, and A. H. MacDonald, Nat. Phys. **14**, 242 (2018).
[2] Y. Tokura, K. Yasuda, and A. Tsukazaki, Nat. Rev. Phys. **1**, 126 (2019).
[3] R. S. K. Mong, A. M. Essin, and J. E. Moore, Phys. Rev. B **81**, 245209 (2010).
[4] C. Fang, M. J. Gilbert, and B. A. Bernevig, Phys. Rev. B **88**, 085406 (2013).
[5] A. A. Burkov and L. Balents, Phys. Rev. Lett. **107**, 127205 (2011).
[6] M. M. Otrokov, I. I. Klimovskikh, H. Bentmann, D. Estyunin, A. Zeugner, Z. S. Aliev, S. Gaß, A. U. B. Wolter, A. V. Koroleva, A. M. Shikin, M. Blanco-Rey, M. Hoffmann, I. P. Rusinov, A. Yu. Vyazovskaya, S. V. Eremeev, Yu. M. Koroteev, V. M. Kuznetsov, F. Freyse, J. Sánchez-Barriga, I. R. Amiraslanov *et al.*, Nature (London) **576**, 416 (2019).
[7] M. M. Otrokov, I. P. Rusinov, M. Blanco-Rey, M. Hoffmann, A. Y. Vyazovskaya, S. V. Eremeev, A. Ernst, P. M. Echenique, A. Arnau, and E. V. Chulkov, Phys. Rev. Lett. **122**, 107202 (2019).
[8] J. Li, Y. Li, S. Du, Z. Wang, B.-L. Gu, S.-C. Zhang, K. He, W. Duan, and Y. Xu, Sci. Adv. **5**, eaaw5685 (2019).
[9] D. Zhang, M. Shi, T. Zhu, D. Xing, H. Zhang, and J. Wang, Phys. Rev. Lett. **122**, 206401 (2019).
[10] H. Sun, B. Xia, Z. Chen, Y. Zhang, P. Liu, Q. Yao, H. Tang, Y. Zhao, H. Xu, and Q. Liu, Phys. Rev. Lett. **123**, 096401 (2019).
[11] J. Ge, Y. Liu, J. Li, H. Li, T. Luo, Y. Wu, Y. Xu, and J. Wang, Natl. Sci. Rev. **7**, 1280 (2020).
[12] Y. Deng, Y. Yu, M. Z. Shi, Z. Guo, Z. Xu, J. Wang, X. H. Chen, and Y. Zhang, Science **367**, 895 (2020).
[13] C. Liu, Y. Wang, H. Li, Y. Wu, Y. Li, J. Li, K. He, Y. Xu, J. Zhang, and Y. Wang, Nat. Mater. **19**, 522 (2020).

[14] C. Liu, Y. Wang, M. Yang, J. Mao, H. Li, Y. Li, J. Li, H. Zhu, J. Wang, L. Li, Y. Wu, Y. Xu, J. Zhang, and Y. Wang, Nat. Commun. **12**, 4647 (2021).
[15] H. Deng, Z. Chen, A. Wołoś, M. Konczykowski, K. Sobczak, J. Sitnicka, I. V. Fedorchenko, J. Borysiuk, T. Heider, L. Pluciński, K. Park, A. B. Georgescu, J. Cano, and L. Krusin-Elbaum, Nat. Phys. **17**, 36 (2021).
[16] X.-L. Qi, T. L. Hughes, and S.-C. Zhang, Phys. Rev. B **78**, 195424 (2008).
[17] N. Varnava and D. Vanderbilt, Phys. Rev. B **98**, 245117 (2018).
[18] B. Chen, F. Fei, D. Zhang, B. Zhang, W. Liu, S. Zhang, P. Wang, B. Wei, Y. Zhang, Z. Zuo, J. Guo, Q. Liu, Z. Wang, X. Wu, J. Zong, X. Xie, W. Chen, Z. Sun, S. Wang, Y. Zhang *et al.*, Nat. Commun. **10**, 4469 (2019).
[19] D. M. Nenno, C. A. C. Garcia, J. Gooth, C. Felser, and P. Narang, Nat. Rev. Phys. **2**, 682 (2020).
[20] A. Sekine and K. Nomura, J. Appl. Phys. **129**, 141101 (2021).
[21] H. Wang, D. Wang, Z. Yang, M. Shi, J. Ruan, D. Xing, J. Wang, and H. Zhang, Phys. Rev. B **101**, 081109(R) (2020).
[22] N. H. Jo, L.-L. Wang, R.-J. Slager, J. Yan, Y. Wu, K. Lee, B. Schrunk, A. Vishwanath, and A. Kaminski, Phys. Rev. B **102**, 045130 (2020).
[23] A. Gao, Y.-F. Liu, C. Hu, J.-X. Qiu, C. Tzschaschel, B. Ghosh, S.-C. Ho, D. Bérubé, R. Chen, H. Sun, Z. Zhang, X.-Y. Zhang, Y.-X. Wang, N. Wang, Z. Huang, C. Felser, A. Agarwal, T. Ding, H.-J. Tien, A. Akey *et al.*, Nature (London) **595**, 521 (2021).
[24] M. Gu, J. Li, H. Sun, Y. Zhao, C. Liu, J. Liu, H. Lu, and Q. Liu, Nat. Commun. **12**, 3524 (2021).
[25] R. C. Vidal, H. Bentmann, T. R. F. Peixoto, A. Zeugner, S. Moser, C.-H. Min, S. Schatz, K. Kißner, M. Ünzelmann, C. I. Fornari, H. B. Vasili, M. Valvidares, K. Sakamoto, D. Mondal, J. Fujii, I. Vobornik, S. Jung, C. Cacho, T. K. Kim, R. J. Koch *et al.*, Phys. Rev. B **100**, 121104(R) (2019).
[26] S. H. Lee, Y. Zhu, Y. Wang, L. Miao, T. Pillsbury, H. Yi, S. Kempinger, J. Hu, C. A. Heikes, P. Quarterman, W. Ratcliff, J. A. Borchers, H. Zhang, X. Ke, D. Graf, N. Alem, C.-Z. Chang, N. Samarth, and Z. Mao, Phys. Rev. Res. **1**, 012011(R) (2019).
[27] A. Zeugner, F. Nietschke, A. U. B. Wolter, S. Gaß, R. C. Vidal, T. R. F. Peixoto, D. Pohl, C. Damm, A. Lubk, R. Hentrich, S. K. Moser, C. Fornari, C. H. Min, S. Schatz, K. Kißner, M. Ünzelmann, M. Kaiser, F. Scaravaggi, B. Rellinghaus, K. Nielsch *et al.*, Chem. Mater. **31**, 2795 (2019).
[28] Y. J. Chen, L. X. Xu, J. H. Li, Y. W. Li, H. Y. Wang, C. F. Zhang, H. Li, Y. Wu, A. J. Liang, C. Chen, S.-W. Jung, C. Cacho, Y.-H. Mao, S. Liu, M.-X. Wang, Y.-F. Guo, Y. Xu, Z.-K. Liu, L.-X. Yang, and Y.-L. Chen, Phys. Rev. X **9**, 041040 (2019).
[29] Y.-J. Hao, P. Liu, Y. Feng, X.-M. Ma, E. F. Schwier, M. Arita, S. Kumar, C. Hu, R. Lu, M. Zeng, Y. Wang, Z. Hao, H.-Y. Sun, K. Zhang, J. Mei, N. Ni, L. Wu, K. Shimada, C. Chen, Q. Liu *et al.*, Phys. Rev. X **9**, 041038 (2019).
[30] H. Li, S.-Y. Gao, S.-F. Duan, Y.-F. Xu, K.-J. Zhu, S.-J. Tian, J.-C. Gao, W.-H. Fan, Z.-C. Rao, J.-R. Huang, J.-J. Li, D.-Y. Yan, Z.-T. Liu, W.-L. Liu, Y.-B. Huang, Y.-L. Li, Y. Liu, G.-B. Zhang, P. Zhang, T. Kondo *et al.*, Phys. Rev. X **9**, 041039 (2019).
[31] P. Swatek, Y. Wu, L.-L. Wang, K. Lee, B. Schrunk, J. Yan, and A. Kaminski, Phys. Rev. B **101**, 161109(R) (2020).
[32] D. Nevola, H. X. Li, J.-Q. Yan, R. G. Moore, H.-N. Lee, H. Miao, and P. D. Johnson, Phys. Rev. Lett. **125**, 117205 (2020).
[33] Z. Liang, A. Luo, M. Shi, Q. Zhang, S. Nie, J. J. Ying, J.-F. He, T. Wu, Z. Wang, G. Xu, Z. Wang, and X.-H. Chen, Phys. Rev. B **102**, 161115(R) (2020).
[34] Y. Hu, L. Xu, M. Shi, A. Luo, S. Peng, Z. Y. Wang, J. J. Ying, T. Wu, Z. K. Liu, C. F. Zhang, Y. L. Chen, G. Xu, X.-H. Chen, and J.-F. He, Phys. Rev. B **101**, 161113(R) (2020).
[35] A. M. Shikin, D. A. Estyunin, N. L. Zaitsev, D. Glazkova, I. I. Klimovskikh, S. O. Filnov, A. G. Rybkin, E. F. Schwier, S. Kumar, A. Kimura, N. Mamedov, Z. Aliev, M. B. Babanly, K. Kokh, O. E. Tereshchenko, M. M. Otrokov, E. V. Chulkov, K. A. Zvezdin, and A. K. Zvezdin, Phys. Rev. B **104**, 115168 (2021).
[36] F. Hou, Q. Yao, C.-S. Zhou, X.-M. Ma, M. Han, Y.-J. Hao, X. Wu, Y. Zhang, H. Sun, C. Liu, Y. Zhao, Q. Liu, and J. Lin, ACS Nano **14**, 11262 (2020).
[37] Y. Zhao and Q. Liu, Appl. Phys. Lett. **119**, 060502 (2021).
[38] M. Garnica, M. M. Otrokov, P. C. Aguilar, I. I. Klimovskikh, D. Estyunin, Z. S. Aliev, I. R. Amiraslanov, N. A. Abdullayev, V. N. Zverev, M. B. Babanly, N. T. Mamedov, A. M. Shikin, A. Arnau, A. L. Vázquez de Parga, E. V. Chulkov, and R. Miranda, npj Quantum Mater. **7**, 7 (2022).
[39] Y. Yuan, X. Wang, H. Li, J. Li, Y. Ji, Z. Hao, Y. Wu, K. He, Y. Wang, Y. Xu, W. Duan, W. Li, and Q.-K. Xue, Nano Lett. **20**, 3271 (2020).
[40] H.-P. Sun, C. M. Wang, S.-B. Zhang, R. Chen, Y. Zhao, C. Liu, Q. Liu, C. Chen, H.-Z. Lu, and X. C. Xie, Phys. Rev. B **102**, 241406(R) (2020).
[41] A. M. Shikin, D. A. Estyunin, I. I. Klimovskikh, S. O. Filnov, E. F. Schwier, S. Kumar, K. Miyamoto, T. Okuda, A. Kimura, K. Kuroda, K. Yaji, S. Shin, Y. Takeda, Y. Saitoh, Z. S. Aliev, N. T. Mamedov, I. R. Amiraslanov, M. B. Babanly, M. M. Otrokov, S. V. Eremeev *et al.*, Sci. Rep. **10**, 13226 (2020).
[42] M. Du, J. Yan, V. R. Cooper, and M. Eisenbach, Adv. Funct. Mater. **31**, 2006516 (2021).
[43] W. Chen, Y. Zhao, Q. Yao, J. Zhang, and Q. Liu, Phys. Rev. B **103**, L201102 (2021).
[44] X.-M. Ma, Z. Chen, E. F. Schwier, Y. Zhang, Y.-J. Hao, S. Kumar, R. Lu, J. Shao, Y. Jin, M. Zeng, X.-R. Liu, Z. Hao, K. Zhang, W. Mansuer, C. Song, Y. Wang, B. Zhao, C. Liu, K. Deng, J. Mei *et al.*, Phys. Rev. B **102**, 245136 (2020).
[45] C. Yan, S. Fernandez-Mulligan, R. Mei, S. H. Lee, N. Protic, R. Fukumori, B. Yan, C. Liu, Z. Mao, and S. Yang, Phys. Rev. B **104**, L041102 (2021).
[46] P. M. Sass, J. Kim, D. Vanderbilt, J. Yan, and W. Wu, Phys. Rev. Lett. **125**, 037201 (2020).
[47] M. Chen, G.-C. Guo, and L. He, J. Phys.: Condens. Matter **22**, 445501 (2010).
[48] P. Li, X. Liu, M. Chen, P. Lin, X. Ren, L. Lin, C. Yang, and L. He, Comput. Mater. Sci. **112**, 503 (2016).
[49] J. P. Perdew, K. Burke, and M. Ernzerhof, Phys. Rev. Lett. **77**, 3865 (1996).
[50] S. Grimme, J. Antony, S. Ehrlich, and H. Krieg, J. Chem. Phys. **132**, 154104 (2010).
[51] S. L. Dudarev, G. A. Botton, S. Y. Savrasov, C. J. Humphreys, and A. P. Sutton, Phys. Rev. B **57**, 1505 (1998).
[52] X. Qu, P. Xu, H. Jiang, L. He, and X. Ren, J. Chem. Phys. **156**, 234104 (2022).
[53] D. R. Hamann, Phys. Rev. B **88**, 085117 (2013).

[54] G. Theurich and N. A. Hill, Phys. Rev. B **64**, 073106 (2001).
[55] M. van Setten, M. Giantomassi, E. Bousquet, M. Verstraete, D. Hamann, X. Gonze, and G.-M. Rignanese, Comput. Phys. Commun. **226**, 39 (2018).
[56] D. S. Lee, T.-H. Kim, C.-H. Park, C.-Y. Chung, Y. S. Lim, W.-S. Seo, and H.-H. Park, CrystEngComm **15**, 5532 (2013).
[57] Z. S. Aliev, I. R. Amiraslanov, D. I. Nasonova, A. V. Shevelkov, N. A. Abdullayev, Z. A. Jahangirli, E. N. Orujlu, M. M. Otrokov, N. T. Mamedov, M. B. Babanly, and E. V. Chulkov, J. Alloys Compd. **789**, 443 (2019).
[58] J.-Q. Yan, Q. Zhang, T. Heitmann, Z. Huang, K. Y. Chen, J.-G. Cheng, W. Wu, D. Vaknin, B. C. Sales, and R. J. McQueeney, Phys. Rev. Mater. **3**, 064202 (2019).
[59] J.-Q. Yan, S. Okamoto, M. A. McGuire, A. F. May, R. J. McQueeney, and B. C. Sales, Phys. Rev. B **100**, 104409 (2019).
[60] B. Li, J.-Q. Yan, D. M. Pajerowski, E. Gordon, A.-M. Nedić, Y. Sizyuk, L. Ke, P. P. Orth, D. Vaknin, and R. J. McQueeney, Phys. Rev. Lett. **124**, 167204 (2020).
[61] Z. Dai, G. Jin, and L. He, Comput. Mater. Sci. **213**, 111656 (2022).
[62] See Supplemental Material at http://link.aps.org/supplemental/10.1103/PhysRevB.108.085112 for a detailed description of the band-unfolding method used in this paper. We also show the layer-decomposed density of states of the surface state and the unfolded spectra of the surface states under different surface magnetizations. It includes citations of Refs. [61,73–77].
[63] R. Yu, W. Zhang, H.-J. Zhang, S.-C. Zhang, X. Dai, and Z. Fang, Science **329**, 61 (2010).
[64] V. N. Men'shov, I. A. Shvets, and E. V. Chulkov, Phys. Rev. B **106**, 205301 (2022).
[65] H. Tan and B. Yan, Phys. Rev. Lett. **130**, 126702 (2023).
[66] Z. Huang, M.-H. Du, J. Yan, and W. Wu, Phys. Rev. Mater. **4**, 121202(R) (2020).
[67] J. Li, C. Wang, Z. Zhang, B.-L. Gu, W. Duan, and Y. Xu, Phys. Rev. B **100**, 121103(R) (2019).
[68] J. Wu, F. Liu, M. Sasase, K. Ienaga, Y. Obata, R. Yukawa, K. Horiba, H. Kumigashira, S. Okuma, T. Inoshita, and H. Hosono, Sci. Adv. **5**, eaax9989 (2019).
[69] Y. Hou and R. Wu, Nano Lett. **19**, 2472 (2019).
[70] H. Fu, C.-X. Liu, and B. Yan, Sci. Adv. **6**, eaaz0948 (2020).
[71] Y. S. Hou, J. W. Kim, and R. Q. Wu, Phys. Rev. B **101**, 121401(R) (2020).
[72] N. Pournaghavi, M. F. Islam, R. Islam, C. Autieri, T. Dietl, and C. M. Canali, Phys. Rev. B **103**, 195308 (2021).
[73] T. G. Dargam, R. B. Capaz, and B. Koiller, Phys. Rev. B **56**, 9625 (1997).
[74] L.-W. Wang, L. Bellaiche, S.-H. Wei, and A. Zunger, Phys. Rev. Lett. **80**, 4725 (1998).
[75] T. B. Boykin and G. Klimeck, Phys. Rev. B **71**, 115215 (2005).
[76] T. B. Boykin, N. Kharche, G. Klimeck, and M. Korkusinski, J. Phys.: Condens. Matter **19**, 036203 (2007).
[77] W. Ku, T. Berlijn, and C.-C. Lee, Phys. Rev. Lett. **104**, 216401 (2010).